ASIAN JOURNAL OF CIVIL ENGINEERING (BHRC) VOL. 14, NO. 1 (2013)
PAGES 161-179

IN-PLANE NUMERICAL MODELLING OF STERNGTHENED PERFORATED MASONRY WALLS USING FRP UNDER CYCLIC LOADING

M.Z. Kabir* and A. Kalali
Department of Civil Engineering, Amirkabir University of Technology (Tehran Polytechnic), Tehran, Iran

Received: 12 January 2012; **Accepted**: 10 May 2012

ABSTRACT

A large inventory of older masonry buildings exists in earthquake-prone regions. The majority of these buildings were built before any provisions for earthquake loading were established. Several seismic retrofitting techniques for masonry structures have been developed and practiced and fiber reinforced polymer (FRP) material has been increasingly used owing to its high strength/stiffness to mass ratio and easy application. This paper presents a finite element modeling approach, developed with commercial software, for the analysis of the behaviour of unreinforced and FRP strengthened perforated brick shear walls when they are subjected to a combination of vertical compression preload and in-plane cyclic shear loading. The numerical simulations are compared with experimental data and the accuracy of the proposed finite element model is validated. Finally, effects of different strengthening configurations with FRP on the in-plane cyclic performance of brick walls with openings (e.g. door, window) having different aspect ratios and positions are examined.

Keywords: Unreinforced brick walls; openings; cyclic behavior; strengthening; fiber reinforced polymers

1. INTRODUCTION

A large number of unreinforced masonry (URM) buildings in the world are seismically vulnerable by today's standards. The failures and damages reported in recent earthquakes attest to the need for efficient strengthening procedures. The main structural elements that resist earthquakes in these buildings are the old unreinforced masonry walls which were designed to resist mainly gravity loads. Under seismic loading, unreinforced masonry walls

* E-mail address of the corresponding author: mzkabir@aut.ac.ir (M.Z. Kabir)

have two possible failure mechanisms, namely in-plane and out-of-plane. In order to preserve these buildings, rehabilitation is often considered essential to maintain their capability and to increase safety. In the last decade, fiber reinforced polymer (FRP) composites have been used for strengthening URM walls of masonry buildings.

Various researchers have examined the use of various FRPs to enhance the in-plane performance of masonry walls under monotonic, cyclic or seismic loading. Large increases in both load and displacement capacity were observed, with the amounts depending on the quantity, type and layout of the FRP used. Also, different in-plane failure modes of FRP strengthened masonry walls were reported such as shear failure, flexural failure, FRP rupture, anchorage failure and debonding failure [1-9].

Whereas extensive research has been conducted and reported for retrofitting of reinforced concrete structures using FRP, much less has been reported for retrofitting of URM walls [10]. Also, very small numbers of these researches on the subject of URM walls have been conducted on perforated URM walls [11-12]. The response of masonry shear wall becomes quite complicated, if the wall has openings for functional requirements. Openings have a significant effect on the characteristics of masonry shear walls such as failure mode, strength and ductility [13-15].

Modeling the complex behavior of masonry is a difficult challenge in the finite element analysis of civil engineering structures. In this study, the objective is to establish a methodology for applying computer modeling to unreinforced masonry walls strengthened with FRP laminates. Finite element analysis, as used in structural engineering, determines the behavior of a structure by dividing it into a number of simple elements, each of which has well-defined mechanical and physical properties. Finite element models are developed to simulate the behavior of three recently tested FRP retrofitted URM walls, using the ANSYS program. Comparisons are made for load-deflection plots and cracking patterns, then the accuracy of the proposed model is validated. Modeling simplifications and assumptions developed during this research are presented. Finite element analysis can also be used for parametric studies. Thus with the selected finite element modeling method, the effects of different FRP types and strengthening configurations on the behaviour of various perforated masonry walls are investigated. Conclusions from the current research efforts are included.

2. FINITE ELEMENT MODELING

2.1 Finite element modeling of URM walls

A smeared cracking approach has been introduced using isoparametric formulations to represent the cracked masonry as an orthotropic material. In the smeared cracking approach, cracking of the masonry occurs when the principal tensile stress exceeds the ultimate tensile strength. The elastic modulus of the material is then assumed to be zero in the direction parallel to the principal tensile stress direction. SOLID65 element in the ANSYS finite element program has this capability. This element is capable of cracking in tension and also crushing in compression. The element is defined by eight nodes having three degrees of freedom at each node: translations in the nodal x, y, and z directions. In this element type, William & Warnke criterion for the failure of the concrete is considered.

Finite element analysis with the smeared cracking approach (using SOLID65 element) has been used to simulate the behavior of URM walls. Comparisons between the experimental data and the results from finite element models showed good agreement [16-20]. Thus in this study, SOLID65 element was used to model the masonry.

In SOLID65 element, cracking is permitted in three orthogonal directions at each integration point. If cracking occurs at an integration point, the cracking is modeled through an adjustment of material properties which effectively treats the cracking as a "smeared band" of cracks, rather than discrete cracks. The presence of a crack at an integration point is represented through modification of the stress-strain relations by introducing a plane of weakness in a direction normal to the crack face. Also, a shear transfer coefficient β_t is introduced which represents a shear strength reduction factor for those subsequent loads which induce sliding (shear) across the crack face. If the crack closes, then all compressive stresses normal to the crack plane are transmitted across the crack and only a shear transfer coefficient β_c for a closed crack is introduced. According to the literature [16-20] and experimental observations, shear transfer coefficients of β_t and β_c, are considered as 0.25 and 0.7, respectively.

2.2 Finite element modeling of FRP retrofitted URM walls

FRP composites are materials that consist of two constituents. The constituents are combined at a macroscopic level and are not soluble in each other. One constituent is the reinforcement, which is embedded in the second constituent, a continuous polymer called the matrix. The reinforcing material is in the form of fibers (e.g. carbon and glass) which are typically stiffer and stronger than the matrix. A one layer FRP laminate has three mutually orthogonal planes of material properties. This material is also transversely isotropic, where the properties are nearly the same in any direction perpendicular to the fibers.

A layered 8-node structural solid element, SOLID46, was used to model the FRP composites. The element allows up to 250 different material layers. The element has three degrees of freedom at each node: translations in the nodal x, y, and z directions. The SOLID46 element is defined by eight nodes, layer thicknesses, layer material direction angles, and orthotropic material properties.

Ideally, the bond strength between the masonry and FRP composites should be considered. However, in this study, perfect bond between materials was assumed. The high strength of the epoxy used to attach FRP sheets to masonry walls supported the perfect bond assumption. In the finite element models, nodes of the FRP layered solid elements were connected to those of adjacent masonry solid elements in order to satisfy the perfect bond assumption.

The FRP composites had different thicknesses at the intersection of the FRP strips. The various thicknesses of the FRP composites create discontinuities, which are not desirable for the finite element analysis. These may develop high stress concentrations at local areas on the models; consequently, when the model is run, the solution may have difficulties in convergence. Therefore, a consistent overall thickness of FRP composite was used in the models to avoid discontinuities. The equivalent overall stiffness of the FRP materials was maintained by making compensating changes in the elastic and shear moduli assigned to each FRP layer. For example, if the thickness of an FRP laminate was artificially doubled to

maintain a constant overall thickness, the elastic and shear moduli in that material were reduced by 50% to compensate.

As an initial step, a finite element analysis requires meshing of the model. In other words, the model is divided into a number of small elements, and after loading, stress and strain are calculated at integration points of these small elements. An important step in finite element modeling is the selection of the mesh density. A convergence of results is obtained when an adequate number of elements is used in a model. This is practically achieved when an increase in the mesh density has a negligible effect on the results. Therefore, in this finite element modeling study a convergence study was carried out to determine an appropriate mesh density [21].

2.3 Comparison with experimental results

In a recent experimental research work, the cyclic behavior of three one-half scale perforated unreinforced brick shear walls before and after strengthening using glass fiber reinforced polymers (GFRPs) was investigated by the authors. This laboratory study was conducted on the existing unreinforced brick shear walls representative of conditions existing in Iran [22]. These walls were constructed using one-half scale solid clay bricks and cement mortar. The original full scale solid clay brick is 210 mm×100 mm×56 mm; this resulted in a ½-scale brick nominally measuring 105 mm×50 mm×28 mm. In addition, during construction the head and bed joints were approximately 6 and 10 mm thick, respectively, to be consistent with the half-scale bricks. The mortar had a composition of 1 part cement to 5 parts sand, by volume. The masonry material properties are summarized in Table 1.

Table 1: Mechanical properties of the masonry materials used in the experimental program

Item	Property	Value
Brick	Compressive strength	11.7 MPa
Mortar	Compressive strength	5.2 MPa
Brick/mortar interface	Tensile bond strength	0.062 MPa
	Shear bond strength	0.2 MPa
	Coefficient of friction	0.58
Masonry prism	Compressive strength	3.89 MPa
	Elastic modulus	843 MPa

Glass fiber reinforced polymers were used to retrofit the brick walls. One brick wall was unreinforced and considered as a reference specimen. Two walls were directly upgraded after construction using one layer of GFRP. Each wall was retrofitted on the surface of both sides. Application of the GFRP took place after curing of the brick walls for at least 28 days in laboratory conditions. The application of the wrap material was a simple and rapid operation. The application method was dry lay-up. An epoxy resin based adhesive (two

component epoxy Sikadur 330) was used for bonding the glass fiber sheet. Cured laminate (GFRP) properties after standard cure are given in Table 2 according to the datasheet made by the manufacturer.

Table 2: GFRP properties used in the experimental program

Tensile strength	Tensile modulus	Tensile elongation	90 deg tensile strength	90 deg tensile modulus	90 deg tensile elongation	Thickness	ASTM test method
537 MPa	26.49 GPa	2.21%	23 MPa	7.07 GPa	0.32%	0.5 mm	D 3039

The length, height and thickness of these walls were 194, 143, and 16 cm, respectively. Thus, the aspect ratio of the test walls was about 0.74. The test walls were constructed on a strong reinforced concrete footing. After allowing the wall to cure (for at least 7 days), a strong reinforced concrete loading beam was built on the top of the brick wall. The foundation and loading beam dimensions were 240 cm×20 cm×24 cm and 194 cm×20 cm×16 cm, respectively. These test walls had a window opening in their center. The length and height of this window were 52 and 47 cm, respectively. The unreinforced and GFRP strengthened walls are illustrated in Figure 1. In specimen RBW-X-S1, the width of the lower and upper diagonal GFRP strips was 15 and 18 cm, respectively. The strengthening of specimen RBW-X-S2 by means of GFRP was relatively similar to specimen RBW-X-S1, but, it had two additional vertical GFRP strips with a width of 15 cm at the beginning and end of the surface of two sides.

(a) (b) (c)

Figure 1. The unreinforced and GFRP strengthened test walls: (a) URBW; (b) RBW-X-S1; (c) RBW-X-S2

In this experimental study, a gravity load of 41.2 kN was applied along the top of the wall by a loading beam in a manner consistent with the floor or roof loading. This vertical load generated an average compression stress of 0.13 MPa and 0.18 MPa in each wall and its piers (adjacent to the window), respectively. For this purpose, a steel loading basket was constructed. This steel loading basket was filled with 210 lead weights and was

subsequently placed on the loading beam. The loading beam distributed this vertical load uniformly on the top of the wall. Thus, this axial load acting on the wall was constant during cyclic loading as seen in the walls in real buildings under seismic loading. Horizontal cyclic load was applied manually in the plane of the wall to the loading beam (via steel plates which were connected to the loading beam during the construction) using two hydraulic jacks and hand pumps. These jacks could only produce compressive load and were mounted on rigid reaction frames. The loading beam distributed this concentrated load uniformly along the top of the wall to simulate floor or roof loads used in the actual masonry building construction. The test wall assembly was laterally supported along its top so as to restrict the out-of-plane displacement of the assembly. The test setup was similar for all of the test walls. For example, it is illustrated in Figure 2 for specimen RBW-X-S1.

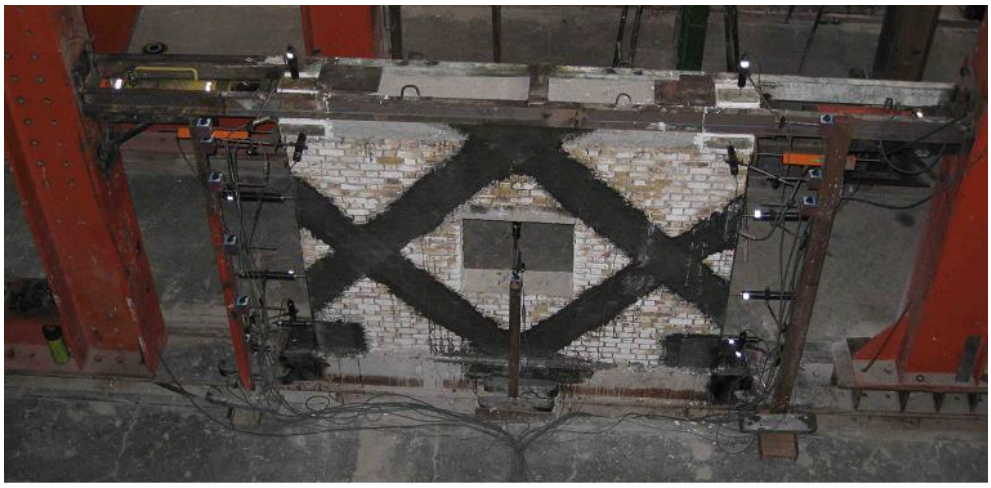

(a)

(b)

Figure 2. Test setup for cyclic load test of specimen RBW-X-S1: (a) Before applying vertical load; (b) After applying vertical load

All these walls were tested under constant gravity load and incrementally increasing in-plane loading cycles according to [23] as shown in Figure 3. The selected loading procedure can simulate the earthquake actions and their effects on the walls. During the test, each wall was allowed to displace in its own plane. The force required to push the wall and the corresponding displacement at each load interval were measured. The observed hysteresis response curve for each tested wall specimen is shown in Figure 3.

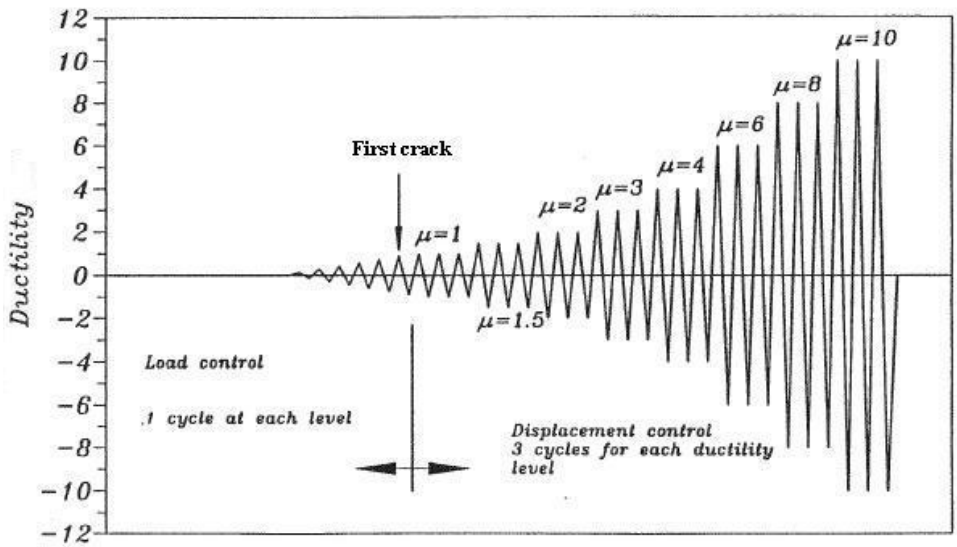

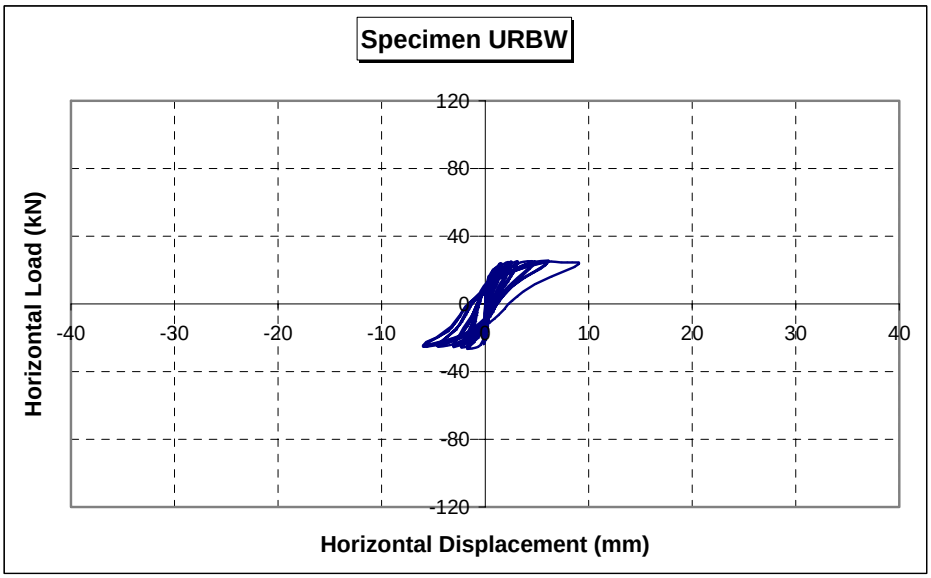

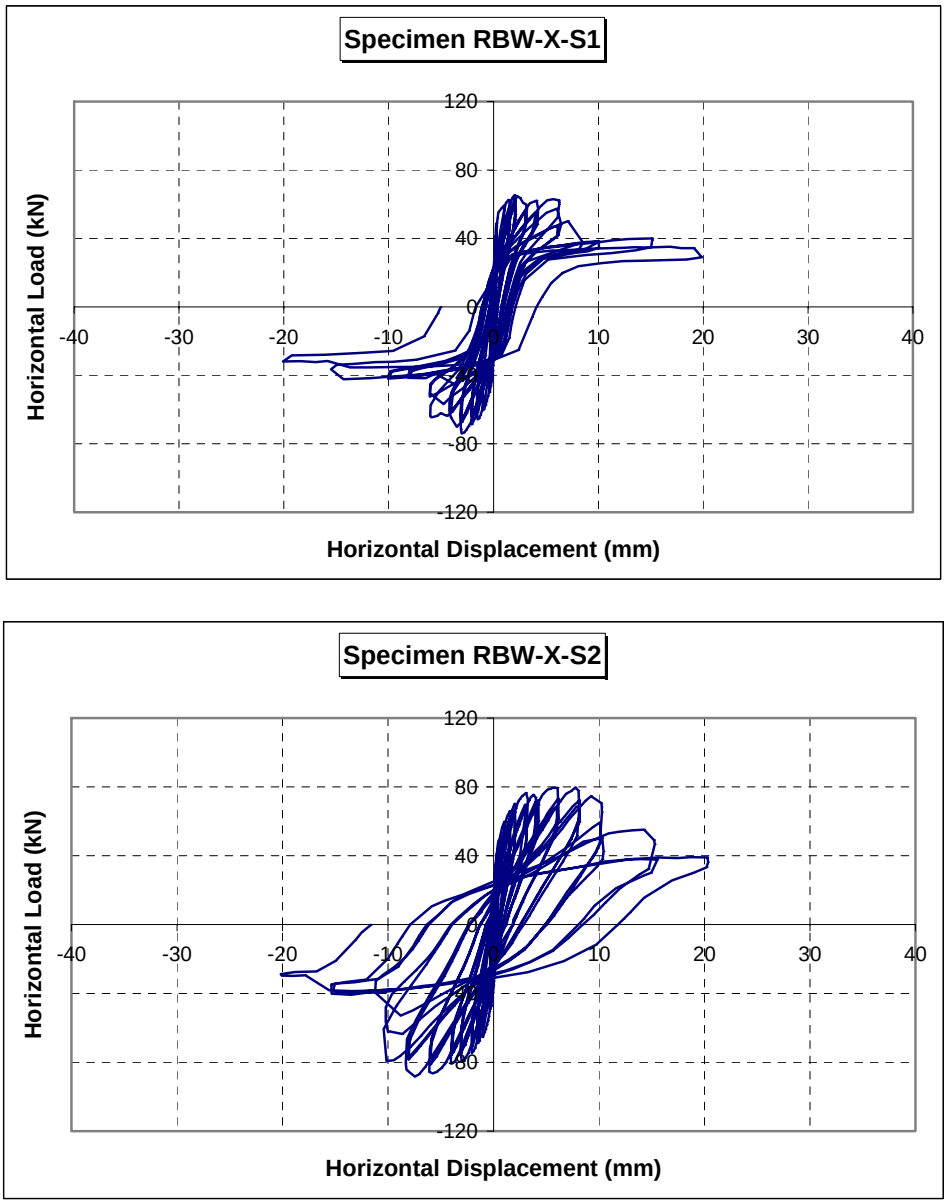

Figure 3. Loading history for the cyclic load test [23] and load-displacement curves at the top of the test walls

The research discussed in this paper – development of computer models to predict the behavior of FRP retrofitted URM walls – uses the data from these walls tests for validation. The ANSYS finite element program was used in this study to simulate the behavior of masonry walls strengthened with FRP laminates as mentioned earlier. Finite element models of specimens URBW, RBW-X-S1 and RBW-X-S2 are presented in Figure 4.

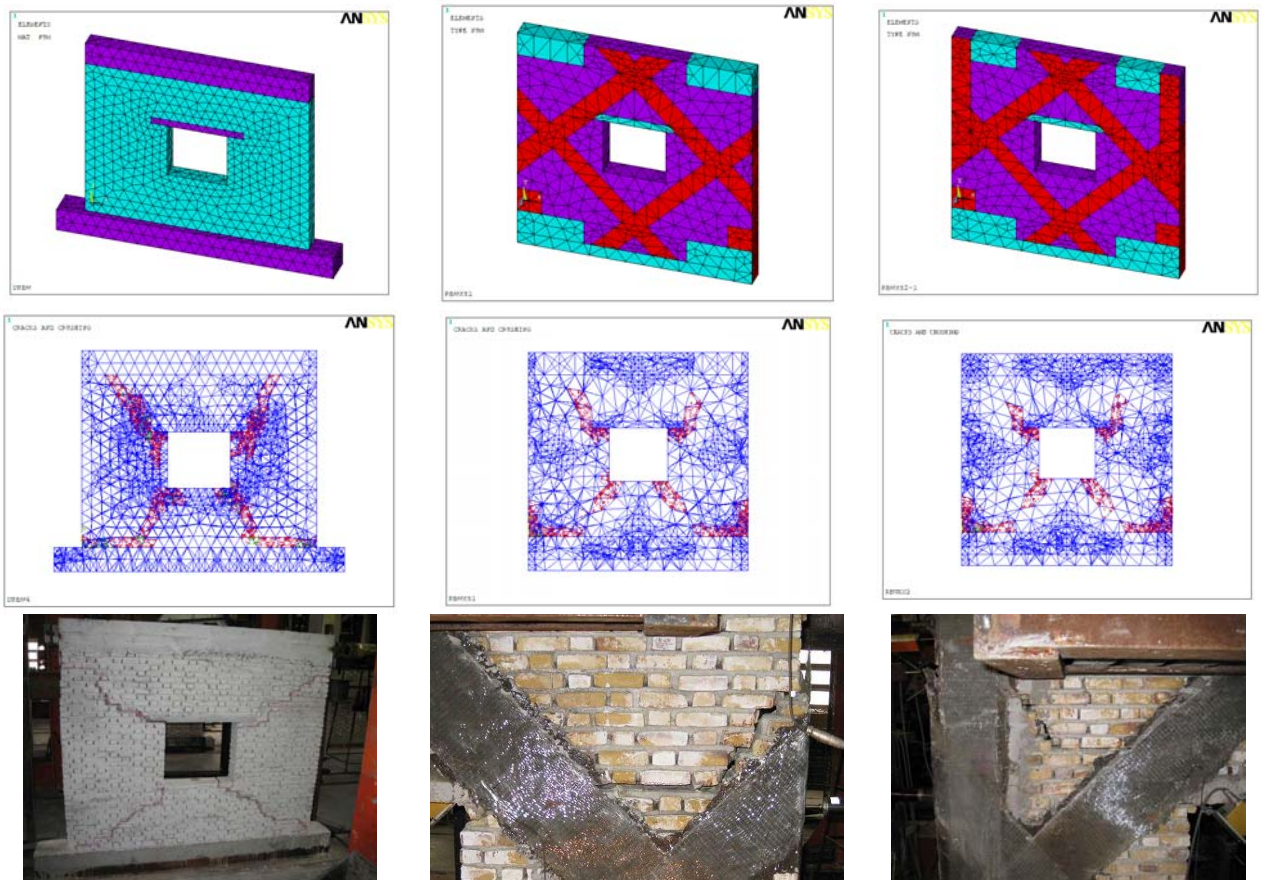

(a) (b) (c)

Figure 4. Finite element model and cracking pattern of the test walls in two cases of numerical and experimental: (a) URBW; (b) RBW-X-S1; (c) RBW-X-S2

Crack patterns obtained from the finite element analyses of the tested walls are shown in Figure 4 which is similar to the experimental observations. The appearance of the cracks defines the failure mode type for the walls. The response of the experimental walls was characterized by the development of early diagonal shear cracks that started at the lower and upper corners of the window and then extended diagonally towards the wall corners. Also, some flexural cracks occurred horizontally in the first bed mortar joint (i.e. between the wall and the foundation) at the toe and heel of the wall. Figures 5-7 show the load-deflection plots from the finite element analyses and the experimental results for all three walls.

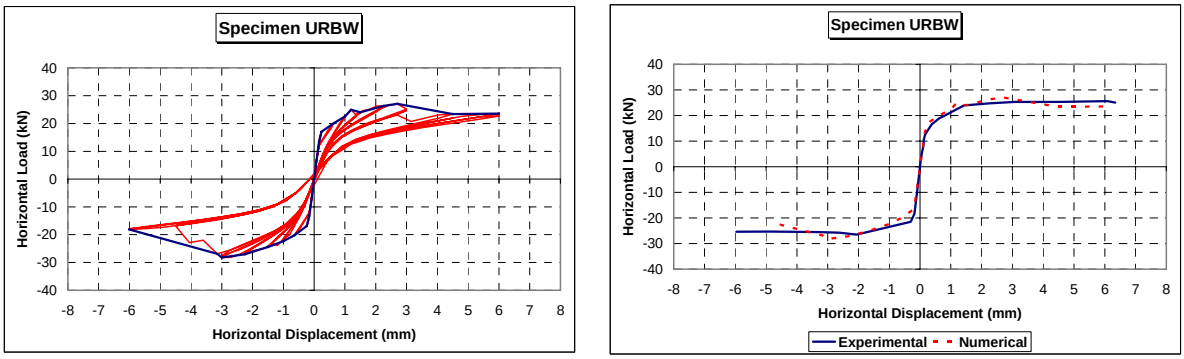

(a) (b)

Figure 5. (a) Numerical hysteresis and envelope curves of specimen URBW; (b) Comparison of numerical and experimental envelope curves of specimen URBW until the failure limit state

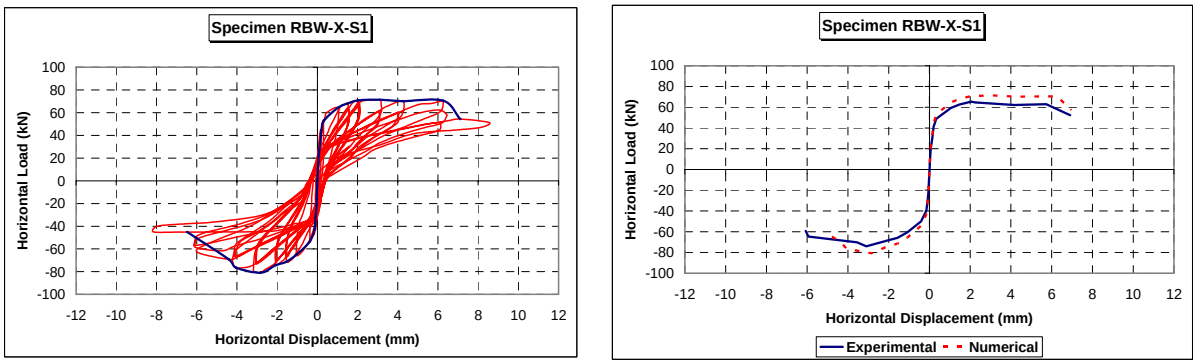

(a) (b)

Figure 6. (a) Numerical hysteresis and envelope curves of specimen RBW-X-S1; (b) Comparison of numerical and experimental envelope curves of specimen RBW-X-S1 until the failure limit state

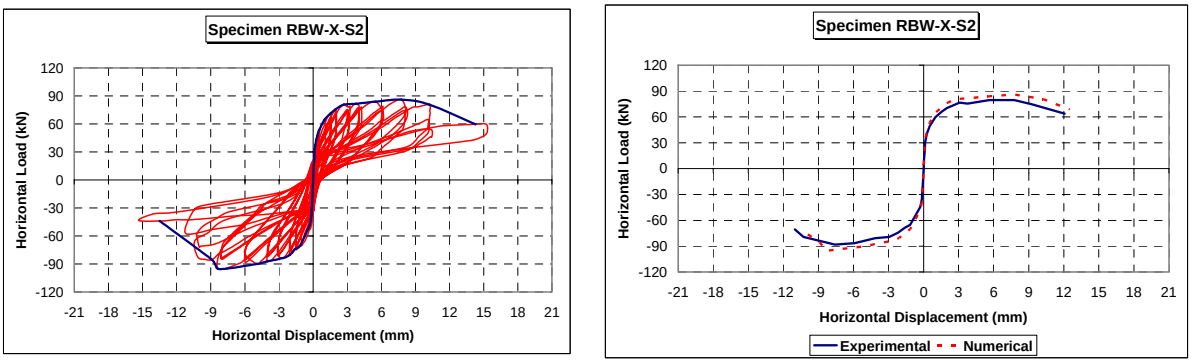

(a) (b)

Figure 7. (a) Numerical hysteresis and envelope curves of specimen RBW-X-S2; (b) Comparison of numerical and experimental envelope curves of specimen RBW-X-S2 until the failure limit state

Figures 5-7 show that the load-deflection plots from the finite element analyses agrees well with the experimental data for the tested walls. The average load-carrying capacities for walls URBW, RBW-X-S1, and RBW-X-S2 from the finite element analyses are higher than those from the experimental results by 6.2%, 9.3%, and 8%, respectively. This is possibly due to the fact that the actual masonry walls contain a number of micro-cracks which were not included in the finite element models. Microcracks generated during the production and constructions are present in the masonry to some degree.

3. DESCRIPTION OF SELECTED MODELS

3.1 Geometry

Selected wall models for the parametric study are shown in Figure 8. The length, height and thickness of these walls were 4.5, 3, and 0.35 m, respectively. The foundation and loading beam dimensions were 4.5 m×0.3 m×0.35 m. In models A, B and E, there was an opening in the center. In models C and D, the distance of the opening edge from the beginning of the wall was 0.75 m. In models A and C, the length and height of the window opening were 1.5 and 1 m, respectively. In models B and D, the length and height of the door opening were 1.2 and 2.2 m, respectively. In model E, the length and height of the window opening were 2.25 and 2 m, respectively.

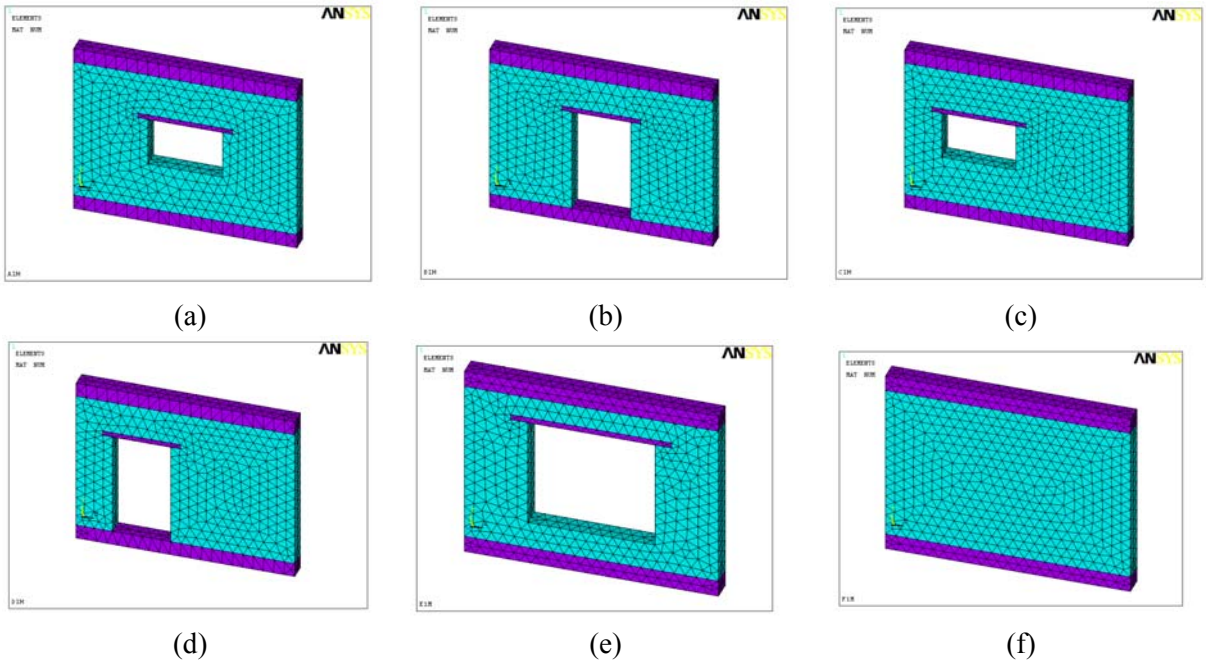

Figure 8. Selected models for the parametric study: (a) model A; (b) model B; (c) model C; (d) model D; (e) model E; (f) model F

3.2 Material properties

The selected properties for the materials are the same as those used in the experimental program as mentioned in the previous section. CFRP properties used in this study are given in Table 3.

Table 3: CFRP properties used in the parametric study

Tensile strength	Tensile modulus	Tensile elongation	90 deg tensile strength	90 deg tensile modulus	90 deg tensile elongation	Thickness	ASTM test method
894 MPa	65.402 GPa	1.37%	27 MPa	5.876 GPa	0.46%	0.5 mm	D 3039

3.3 Strengthening configurations

Reinforcing schemes for the masonry wall models are shown in Figure 9. The walls were reinforced with two layers of FRP that the thickness of each layer was 0.5 mm. The width of the vertical and diagonal FRP strips was 30 cm, except for models B and D which the thickness of the diagonal strips was 35 cm. The width of narrow vertical strips in the case of XII in model B was 15 cm. The vertical and diagonal FRP strips were considered to prevent the walls from uplift and diagonal cracking (shear reinforcement), respectively.

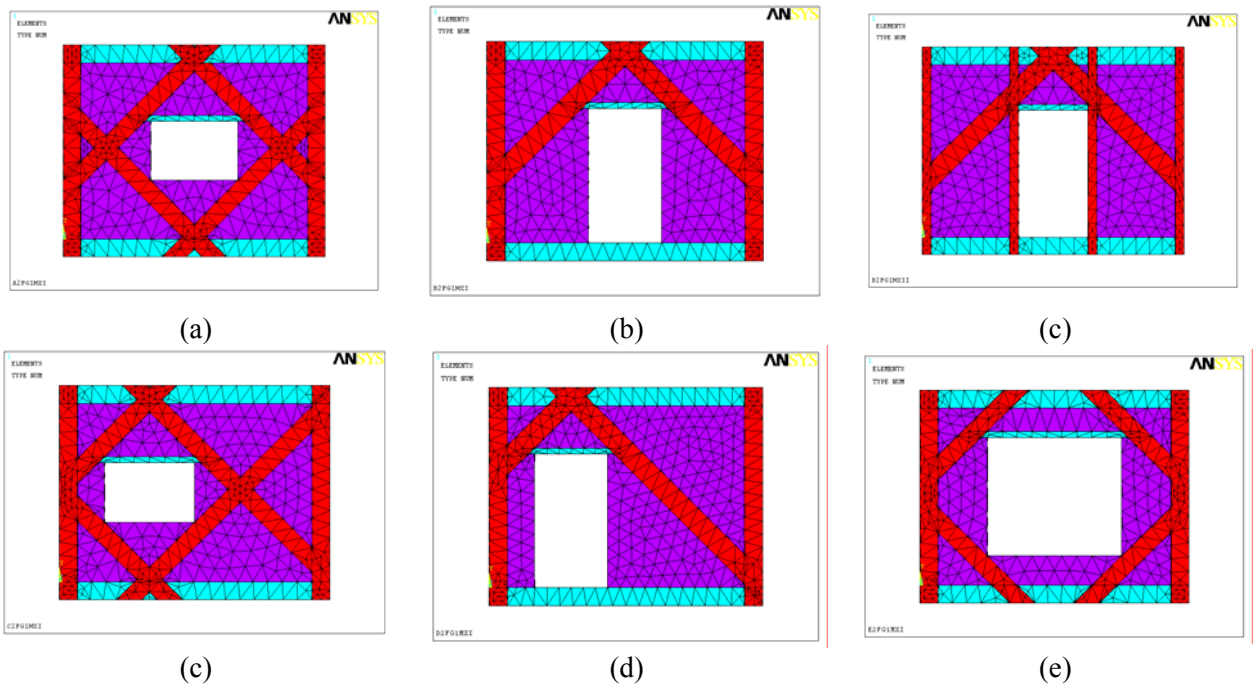

Figure 9. FRP reinforcing schemes for the brick wall models: (a) model A; (b) model B; (c) model C; (d) model D; (e) model E

FRP strengthened walls are denoted by a five letters code where: first letter defines the shape and location of the opening in the wall as mentioned in Figure 8; second is 1F or 2F

depending if FRP strips were installed on one side or two sides of the wall; third is C or G depending if CFRP or GFRP strips were installed; fourth is a symbol depending on the value of the applied gravity stress on the top of the wall (e.g. 1M indicates a gravity stress of 0.1 MPa); fifth is a symbol depending on the FRP pattern.

4. NUMERICAL RESULTS

All the wall finite element models were analyzed under a constant compression preload of 0.1 MPa and in-plane horizontal shear loading cycles. The cyclic load was controlled to follow a cyclic loading sequence as illustrated in Figure 3. Under this loading procedure, Figure 10 shows the crack patterns for each unreinforced wall including flexural and shear cracks. According to Figure 10, it is seen that the flexural failure mode of the solid masonry wall changed into mixed modes of failure, namely shear (diagonal tensile) and flexural due to the opening.

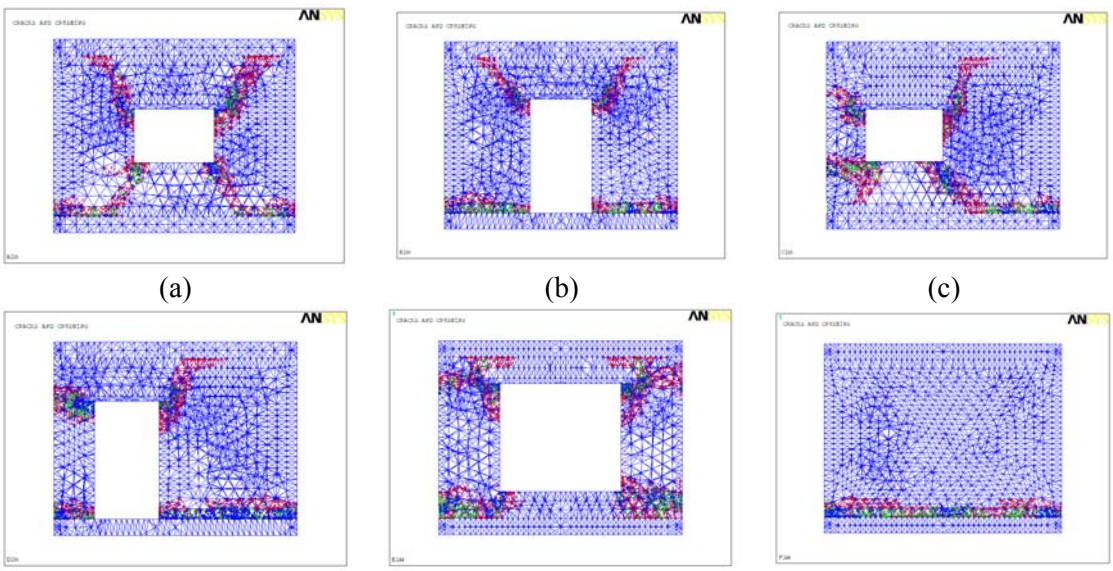

(a) (b) (c)

(d) (e) (f)

Figure 10. Crack patterns at failure: (a) Model A; (b) Model B; (c) Model C; (d) Model D; (e) Model E; (f) Model F

The average cyclic performance parameters were calculated based on envelope curves for solid wall F and corresponding perforated walls, as summarized in Table 4. In addition, the ratio of the average performance parameters of the perforated walls to those of the corresponding solid wall is presented in this table. In Table 4, K_0 is initial stiffness, P_p is maximum load which can be carried by the wall under in-plane cyclic loading and D_u is failure displacement (the displacement at which the applied load based on the envelope curve drops below 80% of the maximum load). According to Table 4, the stiffness and load-bearing capacity of the masonry wall decrease due to the opening; on the other hand the

deformation capacity of the wall increases, because in the perforated walls, the cracks are not concentrated to limited locations (as can be seen in the solid case) but spread in larger areas (Figure 10).

Table 4: Performance parameters of the solid and perforated masonry walls

Wall		K_0 (kN/mm)	P_p (kN)	D_u (mm)
F1M	Average	162.37	241.80	6.65
A1M	Average	113.93	172.59	9.87
	Ratio	0.70	0.71	1.48
B1M	Average	96.91	171.64	13.40
	Ratio	0.60	0.71	2.02
C1M	Average	112.12	177.33	13.56
	Ratio	0.69	0.73	2.04
D1M	Average	97.55	179.91	8.83
	Ratio	0.60	0.74	1.33
E1M	Average	50.24	114.23	12.88
	Ratio	0.31	0.47	1.94

Calculated envelope curves of unreinforced and FRP strengthened walls under cyclic loading are shown in Figures 11-13. Also, the average maximum load and failure displacement are compared in two cases of unreinforced and strengthened with FRP for each type of opening in Table 5.

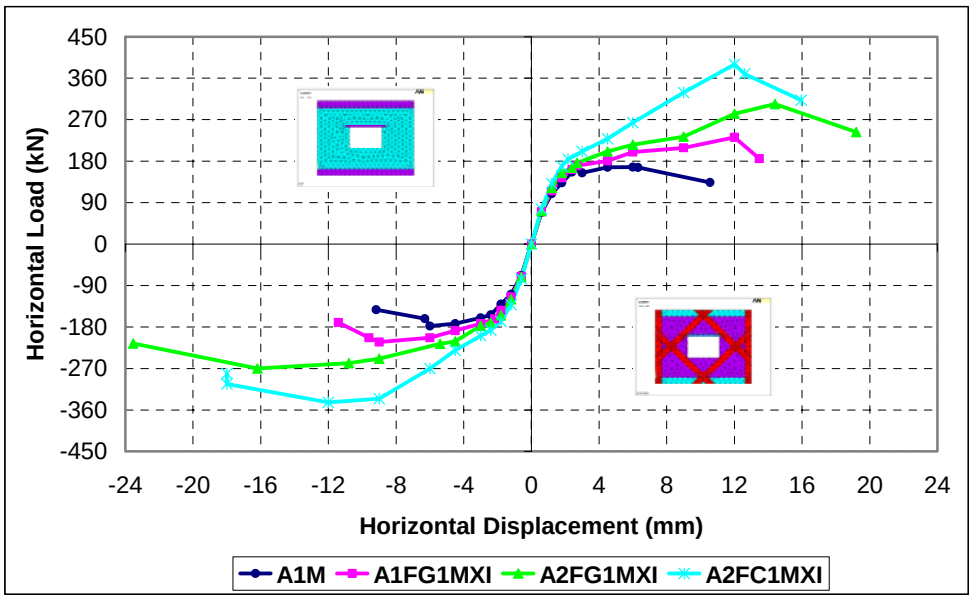

(a)

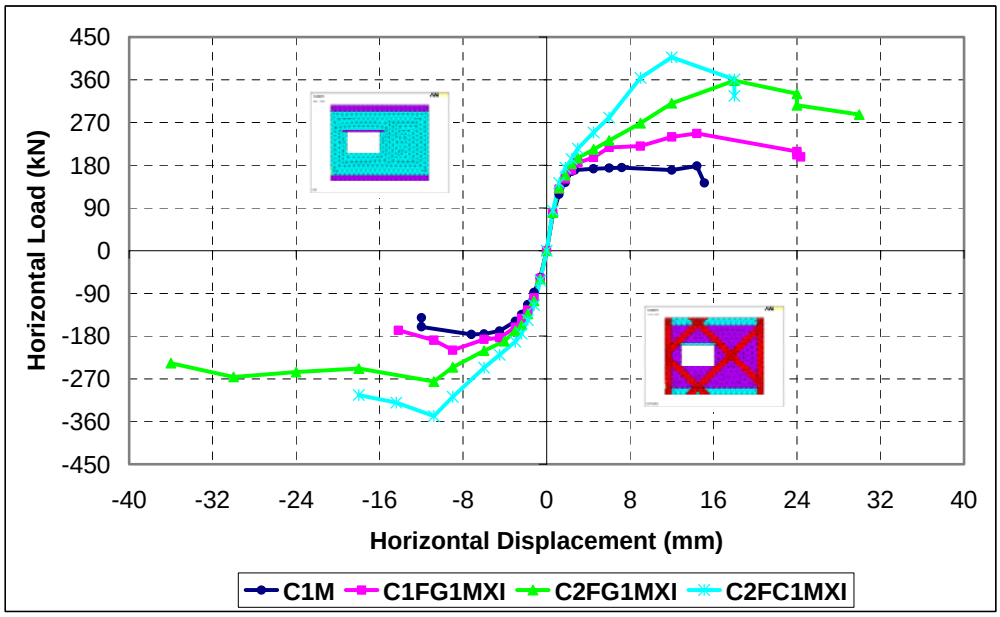

(b)

Figure 11. Comparison of numerical envelope curves until the failure limit state: (a) model A in two cases of unreinforced and strengthened with FRP; (b) model C in two cases of unreinforced and strengthened with FRP

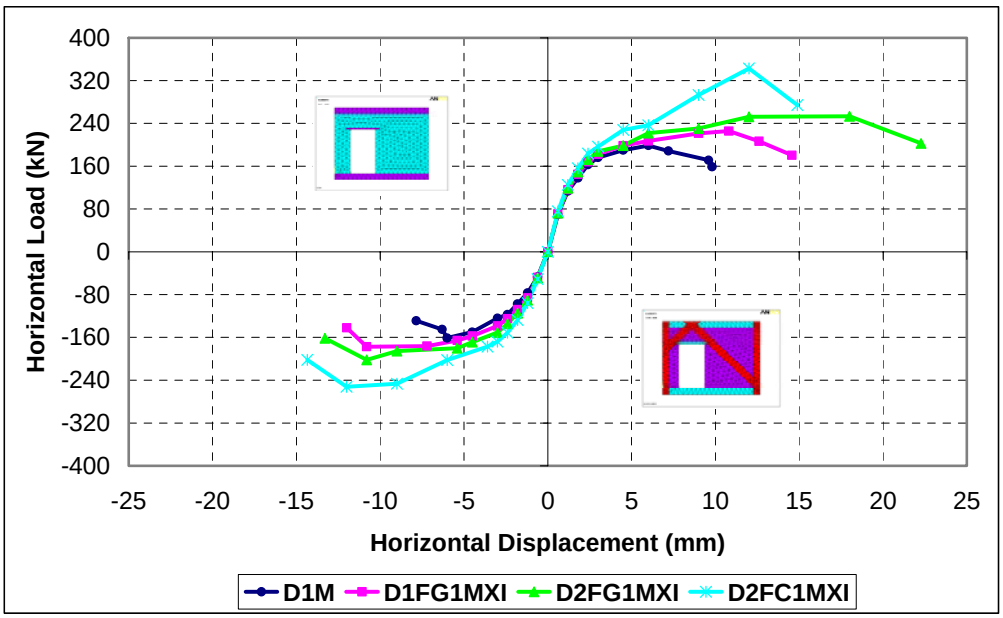

Figure 12. Comparison of numerical envelope curves until the failure limit state for model D in two cases of unreinforced and strengthened with FRP

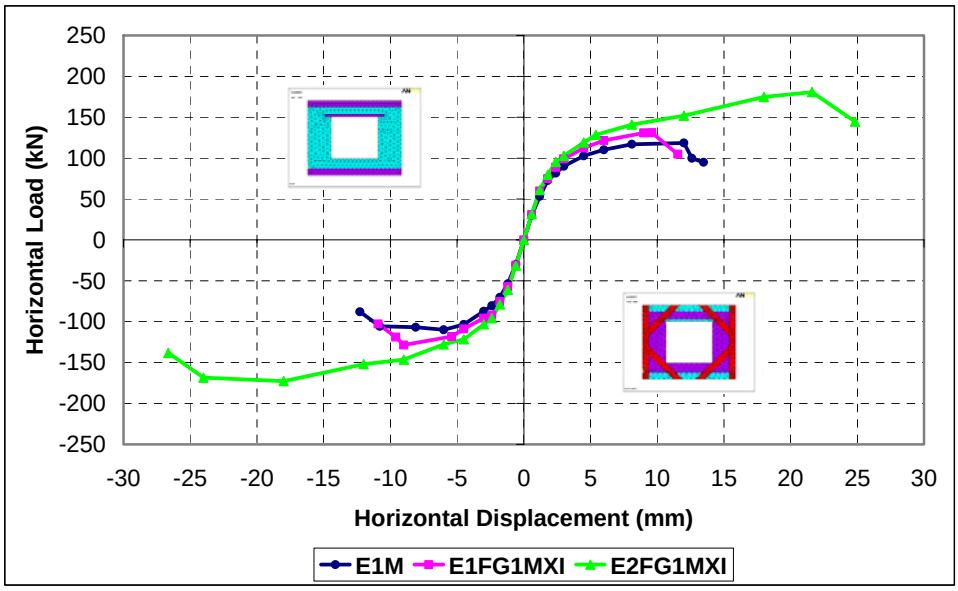

Figure 13. Comparison of numerical envelope curves until the failure limit state for model E in two cases of unreinforced and strengthened with FRP

Table 5: Performance parameters of the investigated walls

Wall		P_p (kN)	D_u (mm)
A1M	Average	172.59	9.87
A1FG1MXI	Average	222.32	12.44
	Ratio	1.29	1.26
A2FG1MXI	Average	286.97	21.37
	Ratio	1.66	2.17
A2FC1MXI	Average	366.77	16.98

Wall		P_p (kN)	D_u (mm)
C1M	Average	177.33	13.56
C1FG1MXI	Average	228.24	19.27
	Ratio	1.29	1.42
C2FG1MXI	Average	317.09	32.98
	Ratio	1.79	2.43
C2FC1MXI	Average	377.98	18.00

Wall		P_p (kN)	D_u (mm)
D1M	Average	179.91	8.83
D1FG1MXI	Average	201.49	13.28
	Ratio	1.12	1.50
D2FG1MXI	Average	227.72	17.78
	Ratio	1.27	2.01
D2FC1MXI	Average	297.62	14.62

Wall		P_p (kN)	D_u(mm)
E1M	Average	114.23	12.88
E2FG1MXI	Average	176.78	25.73
	Ratio	1.55	2.00
E2FC1MXI	Average	209.13	21.23
	Ratio	1.83	1.65

According to Table 5, it can be seen that the increase in the performance parameters is depending on the quantity, type and layout arrangement of the implemented FRP fabrics. CFRP is more efficient in terms of load-bearing capacity than GFRP; but the ductility of CFRP strengthened masonry walls is smaller than that of the corresponding GFRP strengthened masonry walls. In the case of double-side strengthening patterns, the ductility is bigger than that of the corresponding single-side strengthening patterns.

5. CONCLUSIONS

The objective of the current study was to investigate the behaviour of unreinforced and FRP strengthened perforated masonry walls under in-plane cyclic loading. For this purpose, the numerical approach was carried out. The response of three recently tested FRP retrofitted masonry walls were compared to the behaviour predicted by the proposed finite element model here and the accuracy of this model was validated. It was seen that the cyclic performance of a masonry building can be improved significantly by applying FRP sheets to its URM walls. For the particular walls investigated in this study, the following results were obtained:

- The original failure mode of the solid brick wall clearly changed from flexural to mixed failure modes due to the opening. The decrease in the initial stiffness of the solid masonry wall in comparison with the corresponding perforated masonry walls was between 30% and 69%. Also, the decrease in the maximum strength increased from 26% to 53% due to the opening. But, the opening increased the walls' deformation capacity by a factor of 1.33–2.04.
- The load-bearing capacity of the FRP retrofitted perforated masonry walls was between 1.12 and 2.13 times that of the reference unreinforced masonry walls. Also, the FRP increased the failure displacement by a factor ranging from 1.26 to 2.43.

Acknowledgment: The authors would like to express their appreciation and thanks for the technical and financial supports of Iran Building and Housing Research Center (BHRC) in the part of experimental tests.

REFERENCES

1. ElGawady MA, Lestuzzi P, Badoux M. Static cyclic response of masonry walls retrofitted with fiber-reinforced polymers. *Journal of Composites for Construction, ASCE,* **11**(2007) 50–61.
2. Alcaino P, Santa-Maria H. Experimental response of externally retrofitted masonry walls subjected to shear loading. *Journal of Composites for Construction, ASCE,* **12**(2008) 489–98.
3. El-Dakhakhni WW, Hamid AA, Hakam ZHR, Hamelin M. Hazard mitigation and strengthening of unreinforced masonry walls using composites. *Composite Structures* **73**(2006) 458–77.

4. ElGawady MA, Lestuzzi P, Badoux M. In-plane seismic response of URM walls upgraded with FRP. *Journal of Composites for Construction, ASCE* **9**(2005) 524–35.
5. Gabor A, Bennani A, Jacquelin E, Lebon F. Modelling approaches of the in-plane shear behaviour of unreinforced and FRP strengthened masonry panels. *Composite Structures,* **74**(2006) 277–88.
6. Marcari G, Manfredi G, Prota A, Pecce M. In-plane shear performance of masonry panels strengthened with FRP. *Composites Part B: Engineering,* **38**(2007) 887–901.
7. Mosallam A, Banerjee A. Enhancement in in-plane shear capacity of unreinforced masonry (URM) walls strengthened with fiber reinforced polymer composites. *Composites Part B: Engineering,* **42**(2011) 1657–70.
8. Stratford T, Pascale G, Manfroni O, Bonfiglioli B. Shear strengthening masonry panels with sheet glass-fiber reinforced polymer. *Journal of Composites for Construction, ASCE,* **8**(2004) 434–43.
9. Santa-Maria H, Alcaino P. Repair of in-plane shear damaged masonry walls with external FRP. *Construction and Building Materials,* **25**(2011) 1172–80.
10. Shrive NG. The use of fibre reinforced polymers to improve seismic resistance of masonry. *Construction and Building Materials,* **20**(2006) 269–77.
11. Ascione L, Feo L, Fraternali F. Load carrying capacity of 2D FRP/strengthened masonry structures. *Composites Part B: Engineering,* **36**(2005) 619–26.
12. Moon FL, Yi T, Leon RT, Kahn LF. Testing of a full-scale unreinforced masonry building following seismic strengthening. *Journal of Structural Engineering, ASCE,* **133**(2007) 1215–26.
13. Shariq M, Abbas H, Irtaza H, Qamaruddin M. Influence of openings on seismic performance of masonry building walls. *Building and Environment,* **43**(2008) 1232–40.
14. Yi T, Moon FL, Leon RT, Kahn LF. lateral load tests on a two-story unreinforced masonry building. *Journal of Structural Engineering, ASCE,* **132**(2006) 643–52.
15. Yi T, Moon FL, Leon RT, Kahn LF. Analyses of a two-story unreinforced masonry building. *Journal of Structural Engineering, ASCE,* **132**(2006) 653–62.
16. Kabir MZ, Farrin M. Numerical Analysis of in-plane performance of unreinforced masonry walls retrofitted with fiber reinforced polymers, *Proceedings of the Eleventh International Conference on Civil, Structural and Environmental Engineering Computing*, Stirlingshire, Scotland, 2007.
17. Betti M, Vignoli A. Assessment of seismic resistance of a basilica-type church under earthquake loading: Modelling and analysis. *Advances in Engineering Software,* **39**(2008) 258–83.
18. Betti M, Vignoli A. Modelling and analysis of a Romanesque church under earthquake loading: assessment of seismic resistance. *Engineering Structures,* **30**(2008) 352–67.
19. Kappos AJ, Penelis GG, Drakopoulos CG. Evaluation of simplified models for lateral load analysis of unreinforced masonry buildings. *Journal of Structural Engineering, ASCE,* **128**(2002) 890–7.
20. Pallarés FJ, Agüero A, Martín M. Seismic behaviour of industrial masonry chimneys. *International Journal of Solids and Structures,* **43**(2006) 2076–90.

21. Kalali A, Kabir MZ. Modeling of unreinforced brick walls under in-plane shear & compression loading. *Structural Engineering and Mechanics,* **36**(2010) 247–78.
22. Tasnimi AA. Behavior of brick walls recommended by Iranian code of practice for seismic resistant design of buildings, Building and Housing Research Center, No. R-404, Tehran, Iran, 2004.
23. AC 125. Acceptance criteria for concrete and reinforced and unreinforced masonry strengthening using externally bonded fiber-reinforced polymer (FRP) composite systems, ICC Evaluation Service, Inc., 2007.